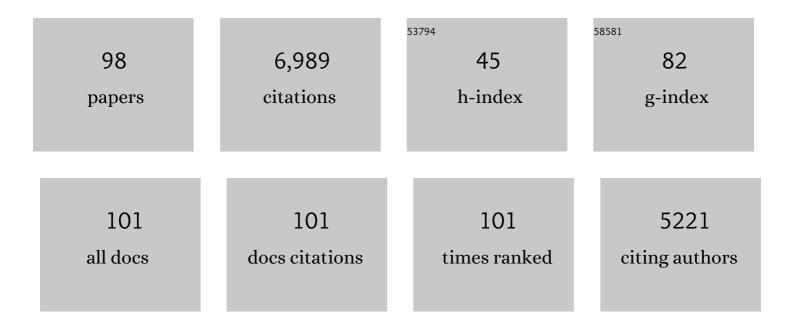
List of Publications by Year in descending order

Source: https://exaly.com/author-pdf/7749324/publications.pdf Version: 2024-02-01



RRUNO LANSON

#	Article	IF	CITATIONS
1	Investigation of smectite hydration properties by modeling experimental X-ray diffraction patterns: Part I. Montmorillonite hydration properties. American Mineralogist, 2005, 90, 1358-1374.	1.9	429
2	Structural model for the biogenic Mn oxide produced by Pseudomonas putida. American Mineralogist, 2006, 91, 489-502.	1.9	288
3	Authigenic kaolin and illitic minerals during burial diagenesis of sandstones: a review. Clay Minerals, 2002, 37, 1-22.	0.6	265
4	Structure of heavy metal sorbed birnessite. Part III: Results from powder and polarized extended X-ray absorption fine structure spectroscopy. Geochimica Et Cosmochimica Acta, 2002, 66, 2639-2663.	3.9	242
5	Structural mechanism of Co (super 2+) oxidation by the phyllomanganate buserite. American Mineralogist, 1997, 82, 1150-1175.	1.9	235
6	Decomposition of Experimental X-ray Diffraction Patterns (Profile Fitting): A Convenient Way to Study Clay Minerals. Clays and Clay Minerals, 1997, 45, 132-146.	1.3	204
7	Structure of H-exchanged hexagonal birnessite and its mechanism of formation from Na-rich monoclinic buserite at low pH. American Mineralogist, 2000, 85, 826-838.	1.9	191
8	Hydration Properties and Interlayer Organization of Water and Ions in Synthetic Na-Smectite with Tetrahedral Layer Charge. Part 1. Results from X-ray Diffraction Profile Modeling. Journal of Physical Chemistry C, 2010, 114, 4515-4526.	3.1	189
9	Site Occupancies by Iron in Nontronites. Clays and Clay Minerals, 2002, 50, 223-239.	1.3	184
10	Structure of Synthetic K-rich Birnessite Obtained by High-Temperature Decomposition of KMnO4. I. Two-Layer Polytype from 800 °C Experiment. Chemistry of Materials, 2003, 15, 4666-4678.	6.7	169
11	Interactions of Oxytetracycline with a Smectite Clay: A Spectroscopic Study with Molecular Simulations. Environmental Science & amp; Technology, 2010, 44, 7839-7845.	10.0	159
12	Natural speciation of Zn at the micrometer scale in a clayey soil using X-ray fluorescence, absorption, and diffraction. Geochimica Et Cosmochimica Acta, 2004, 68, 2467-2483.	3.9	156
13	Investigation of dioctahedral smectite hydration properties by modeling of X-ray diffraction profiles: Influence of layer charge and charge location. American Mineralogist, 2007, 92, 1731-1743.	1.9	156
14	New Insights on the Distribution of Interlayer Water in Bi-Hydrated Smectite from X-ray Diffraction Profile Modeling of 00lReflections. Chemistry of Materials, 2005, 17, 3499-3512.	6.7	154
15	Structure of synthetic Na-birnessite: Evidence for a triclinic one-layer unit cell. American Mineralogist, 2002, 87, 1662-1671.	1.9	152
16	Structure of nanocrystalline phyllomanganates produced by freshwater fungi. American Mineralogist, 2010, 95, 1608-1616.	1.9	138
17	Diagenetic smectite-to-illite transition in clay-rich sediments: A reappraisal of X-ray diffraction results using the multi-specimen method. Numerische Mathematik, 2009, 309, 476-516.	1.4	137
18	Hydration Properties and Interlayer Organization of Water and Ions in Synthetic Na-Smectite with Tetrahedral Layer Charge. Part 2. Toward a Precise Coupling between Molecular Simulations and Diffraction Data. Journal of Physical Chemistry C, 2011, 115, 1867-1881.	3.1	134

#	Article	IF	CITATIONS
19	Characterization of the End of Smectite-to-Illite Transformation: Decomposition of X-ray Patterns. Clays and Clay Minerals, 1992, 40, 40-52.	1.3	119
20	Structure of heavy-metal sorbed birnessite: Part 1. Results from X-ray diffraction. American Mineralogist, 2002, 87, 1631-1645.	1.9	115
21	Birnessite polytype systematics and identification by powder X-ray diffraction. American Mineralogist, 2007, 92, 771-788.	1.9	114
22	Zn sorption modifies dynamically the layer and interlayer structure of vernadite. Geochimica Et Cosmochimica Acta, 2012, 85, 302-313.	3.9	110
23	Kinetic constraints on illitization reactions and the effects of organic diagenesis in sandstone/shale sequences. Applied Geochemistry, 1997, 12, 23-35.	3.0	109
24	Experimental investigation of the interaction of clays with high-pH solutions: A case study from the Callovo-Oxfordian formation, Meuse-Haute Marne underground laboratory (France). Clays and Clay Minerals, 2002, 50, 633-646.	1.3	109
25	Experimental study of smectite interaction with metal Fe at low temperature: 1. Smectite destabilization. Clays and Clay Minerals, 2005, 53, 597-612.	1.3	102
26	Mercury speciation in a tropical soil association; Consequence of gold mining on Hg distribution in French Guiana. Geoderma, 2009, 153, 331-346.	5.1	93
27	On the nature of structural disorder in calcium silicate hydrates with a calcium/silicon ratio similar to tobermorite. Cement and Concrete Research, 2013, 52, 31-37.	11.0	90
28	Structure of Birnessite Obtained from Decomposition of Permanganate under Soft Hydrothermal Conditions. 1. Chemical and Structural Evolution as a Function of Temperature. Chemistry of Materials, 2005, 17, 2959-2975.	6.7	89
29	Clay minerals in the Meuse-Haute Marne underground laboratory (France): Possible influence of organic matter on clay mineral evolution. Clays and Clay Minerals, 2004, 52, 515-532.	1.3	87
30	Formation of Zn–Ca phyllomanganate nanoparticles in grass roots. Geochimica Et Cosmochimica Acta, 2008, 72, 2478-2490.	3.9	74
31	Influence of Tetrahedral Layer Charge on the Organization of Interlayer Water and Ions in Synthetic Na-Saturated Smectites. Journal of Physical Chemistry C, 2015, 119, 4158-4172.	3.1	74
32	Crystal structure of Ni-sorbed synthetic vernadite: a powder X-ray diffraction study. Mineralogical Magazine, 2008, 72, 1279-1291.	1.4	73
33	Structure of the synthetic K-rich phyllomanganate birnessite obtained by high-temperature decomposition of KMnO4. Microporous and Mesoporous Materials, 2007, 98, 267-282.	4.4	72
34	Short-range and long-range order of phyllomanganate nanoparticles determined using high-energy X-ray scattering. Journal of Applied Crystallography, 2013, 46, 193-209.	4.5	70
35	Hydration of Ti <sub>3</sub> C <sub>2</sub> T <i><sub>x</sub></i> MXene: An Interstratification Process with Major Implications on Physical Properties. Chemistry of Materials, 2019, 31, 454-461.	6.7	70
36	Enhanced interlayer trapping of a tetracycline antibiotic within montmorillonite layers in the presence of Ca and Mg. Journal of Colloid and Interface Science, 2016, 464, 153-159.	9.4	64

37	Influence of pH on the interlayer cationic composition and hydration state of Ca-montmorillonite: Analytical chemistry, chemical modelling and XRD profile modelling study. Geochimica Et Cosmochimica Acta, 2005, 69, 2797-2812.	3.9	60
38	Advances in characterization of soil clay mineralogy using Xâ€ray diffraction: from decomposition to profile fitting. European Journal of Soil Science, 2009, 60, 1093-1105.	3.9	56
39	Decomposition of X-ray Diffraction Patterns: A Convenient Way to Describe Complex I/S Diagenetic Evolution. Clays and Clay Minerals, 1992, 40, 629-643.	1.3	55
40	Structure of Synthetic K-Rich Birnessites Obtained by High-Temperature Decomposition of KMnO4. 2. Phase and Structural Heterogeneities. Chemistry of Materials, 2004, 16, 1890-1905.	6.7	53
41	Smectite fluorination and its impact on interlayer water content and structure: A way to fine tune the hydrophilicity of clay surfaces?. Microporous and Mesoporous Materials, 2013, 181, 233-247.	4.4	53
42	Substructure and superstructure of four-layer Ca-exchanged birnessite. American Mineralogist, 1998, 83, 97-118.	1.9	51
43	Solid-state transformation of nanocrystalline phyllomanganate into tectomanganate: influence of initial layer and interlayer structure. Acta Crystallographica Section B: Structural Science, Crystal Engineering and Materials, 2014, 70, 828-838.	1.1	51
44	Crystal growth and aggregation in suspensions of δ-MnO <sub>2</sub> nanoparticles: implications for surface reactivity. Environmental Science: Nano, 2018, 5, 497-508.	4.3	48
45	Experimental investigation of smectite interaction with metal iron at 80 ÂC: Structural characterization of newly formed Fe-rich phyllosilicates. American Mineralogist, 2012, 97, 864-871.	1.9	46
46	Structure of heavy-metal sorbed birnessite: Part 2. Results from electron diffraction. American Mineralogist, 2002, 87, 1646-1661.	1.9	42
47	Experimental evidence for Ca-chloride ion pairs in the interlayer of montmorillonite. An XRD profile modeling approach. Clays and Clay Minerals, 2005, 53, 348-360.	1.3	40
48	Illite-smectite mixed-layer minerals in the hydrothermal alteration of volcanic rocks: I. One-dimensional XRD structure analysis and characterization of component layers. Clays and Clay Minerals, 2005, 53, 423-439.	1.3	39
49	Transformation of Co-containing birnessite to todorokite: Effect of Co on the transformation and implications for Co mobility. Geochimica Et Cosmochimica Acta, 2019, 246, 21-40.	3.9	38
50	Interlayer structure model of tri-hydrated low-charge smectite by X-ray diffraction and Monte Carlo modeling in the Grand Canonical ensemble. American Mineralogist, 2014, 99, 1724-1735.	1.9	37
51	Cryptomelane formation from nanocrystalline vernadite precursor: a high energy X-ray scattering and transmission electron microscopy perspective on reaction mechanisms. Geochemical Transactions, 2015, 16, 12.	0.7	37
52	Selectivity of Na–montmorillonite in relation with the concentration of bivalent cation (Cu2+, Ca2+,) Tj ETQqC	00rgBT	/Oyerlock 10
53	Fast Precipitation of Acicular Goethite from Ferric Hydroxide Gel under Moderate Temperature (30) Tj ETQq1 1 0	.784314 I 3.0	rgBT/Overloc

Rheological properties of clayey soils originating from flow-like landslides. Landslides, 2018, 15, 1615-1630.

5.4 33

#	Article	IF	CITATIONS
55	Phosphorus speciation and micro-scale spatial distribution in North-American temperate agricultural soils from micro X-ray fluorescence and X-ray absorption near-edge spectroscopy. Plant and Soil, 2016, 401, 7-22.	3.7	31
56	Vermiculitization of smectite interfaces and illite layer growth as a possible dual model for illite-smectite illitization in diagenetic environments: a synthesis. Clay Minerals, 2000, 35, 573-586.	0.6	30
57	Illite-smectite mixed-layer minerals in the hydrothermal alteration of volcanic rocks: II. One-dimensional HRTEM structure images and formation mechanisms. Clays and Clay Minerals, 2005, 53, 440-451.	1.3	28
58	Charge location effect on the hydration properties of synthetic saponite and hectorite saturated by Na+, Ca2+ cations: XRD investigation. Applied Clay Science, 2009, 46, 43-50.	5.2	28
59	Interstratification Patterns from the pH-Dependent Intercalation of a Tetracycline Antibiotic within Montmorillonite Layers. Langmuir, 2013, 29, 4492-4501.	3.5	28
60	Comparison of I/S Transformation and Maturity of Organic Matter at Elevated Temperatures. Clays and Clay Minerals, 1993, 41, 178-183.	1.3	26
61	Late-Stage Diagenesis of Illitic Clay Minerals as Seen by Decomposition of X-ray Diffraction Patterns: Contrasted Behaviors of Sedimentary Basins with Different Burial Histories. Clays and Clay Minerals, 1998, 46, 69-78.	1.3	26
62	The smectitic minerals in a bentonite deposit from Melo (Uruguay). Clay Minerals, 2003, 38, 25-34.	0.6	25
63	Experimental aluminization of vermiculite interlayers: An X-ray diffraction perspective on crystal chemistry and structural mechanisms. Geoderma, 2015, 249-250, 28-39.	5.1	25
64	Composition variation of illite-vermiculitesmectite mixed-layer minerals in a bentonite bed from Charente (France). Clay Minerals, 2004, 39, 317-332.	0.6	23
65	The fate of smectite in KOH solutions. American Mineralogist, 2006, 91, 1313-1322.	1.9	23
66	Experimental Study of the Stability and Phase Relations of Clays at High Temperature in a Thermal Gradient. Clays and Clay Minerals, 2012, 60, 200-225.	1.3	21
67	Nucleation and growth of feitknechtite from nanocrystalline vernadite precursor. European Journal of Mineralogy, 2017, 29, 767-776.	1.3	21
68	Chemical signature of two Permian volcanic ash deposits within a bentonite bed from Melo, Uruguay. Anais Da Academia Brasileira De Ciencias, 2006, 78, 525-541.	0.8	19
69	Influence of layer charge on hydration properties of synthetic octahedrally-charged Na-saturated trioctahedral swelling phyllosilicates. Applied Clay Science, 2020, 184, 105404.	5.2	18
70	Highly enhanced oxidation of arsenite at the surface of birnessite in the presence of pyrophosphate and the underlying reaction mechanisms. Water Research, 2020, 187, 116420.	11.3	17
71	Structure of the {001} talc surface as seen by atomic force microscopy: comparison with X-ray and electron diffraction results. European Journal of Mineralogy, 2006, 18, 483-491.	1.3	16
72	Experimental Determinations of the Coherent Scattering Domain Size Distribution of Natural Mica-Like Phases with the Warren-Averbach Technique. Clays and Clay Minerals, 1994, 42, 489-494.	1.3	15

#	Article	IF	CITATIONS
73	Adsorption of Pharmaceuticals onto Smectite Clay Minerals: A Combined Experimental and Theoretical Study. Minerals (Basel, Switzerland), 2021, 11, 62.	2.0	15
74	Mineralogical differences in a temperate cultivated soil arising from different agronomic processes and plant K-uptake. Geoderma, 2019, 347, 210-219.	5.1	14
75	Effects of Mn <sup>2+</sup> , Ni <sup>2+</sup> , and Cu <sup>2+</sup> on the Formation and Transformation of Hydrosulfate Green Rust: Reaction Processes and Underlying Mechanisms. ACS Earth and Space Chemistry, 2019, 3, 519-530.	2.7	14
76	Formation and transformation of schwertmannite through direct Fe <sup>3+</sup> hydrolysis under various geochemical conditions. Environmental Science: Nano, 2020, 7, 2385-2398.	4.3	14
77	Modelling of X-ray diffraction profiles. , 2011, , 151-202.		13
78	Natural organic matter (NOM)-clay association and impact on Callovo-Oxfordian clay stability inÂhigh alkaline solution: Spectromicroscopic evidence. European Physical Journal Special Topics, 2003, 104, 413-416.	0.2	12
79	Influence of the Outer Surface Layers of Crystals on the X-Ray Diffraction Intensity of Basal Reflections. Clays and Clay Minerals, 2004, 52, 680-692.	1.3	12
80	Soil Development under Continuous Agriculture at the Morrow Plots Experimental Fields from X-ray Diffraction Profile Modelling. Soil Systems, 2018, 2, 46.	2.6	12
81	Transformation of the phyllomanganate vernadite to tectomanganates with small tunnel sizes: Favorable geochemical conditions and fate of associated Co. Geochimica Et Cosmochimica Acta, 2021, 295, 224-236.	3.9	12
82	Transformation of Ni-containing birnessite to tectomanganate: Influence and fate of weakly bound Ni(II) species. Geochimica Et Cosmochimica Acta, 2020, 271, 96-115.	3.9	11
83	Classical Polarizable Force Field to Study Hydrated Hectorite: Optimization on DFT Calculations and Validation against XRD Data. Minerals (Basel, Switzerland), 2018, 8, 205.	2.0	10
84	Coupled morphological and structural evolution of δ-MnO <sub>2</sub> to α-MnO <sub>2</sub> through multistage oriented assembly processes: the role of Mn( <scp>iii</scp> ). Environmental Science: Nano, 2020, 7, 238-249.	4.3	10
85	Effects of Co doping on the structure and physicochemical properties of hausmannite (Mn3O4) and its transformation during aging. Chemical Geology, 2021, 582, 120448.	3.3	9
86	Smectite quantification in hydrothermally altered volcanic rocks. Geothermics, 2020, 85, 101748.	3.4	8
87	A quantitative and mechanistic model for the coupling between chemistry and clay hydration. Geochimica Et Cosmochimica Acta, 2020, 283, 124-135.	3.9	8
88	Water Trapping Dynamics in Carbohydrate-Populated Smectite Interlayer Nanopores. Journal of Physical Chemistry C, 2019, 123, 28816-28827.	3.1	5
89	Effects of cobalt doping on the reactivity of hausmannite for As(III) oxidation and As(V) adsorption. Journal of Environmental Sciences, 2022, 122, 217-226.	6.1	5
90	Aluminum extracts in Antarctic paleosols: Proxy data for organic compounds and bacteria and implications for Martian paleosols. Sedimentary Geology, 2011, 237, 84-94.	2.1	4

#	Article	IF	CITATIONS
91	Polytype and polymorph identification of finely divided aluminous dioctahedral mica individual crystals with SAED. Kinematical and dynamical electron diffraction. Physics and Chemistry of Minerals, 2011, 38, 435-448.	0.8	2
92	POLYMORPH AND POLYTYPE IDENTIFICATION FROM INDIVIDUAL MICA PARTICLES USING SELECTED AREA ELECTRON DIFFRACTION. Clays and Clay Minerals, 2020, 68, 334-346.	1.3	2
93	Direct dating of brittle extensional deformation contemporaneous of Neogene exhumation of the internal zones of the Rif Chain. Tectonophysics, 2021, 807, 228800.	2.2	2
94	Characterization and origin of the Mn-rich patinas formed on Lunéville château sandstones. European Journal of Mineralogy, 2021, 33, 687-702.	1.3	2
95	Effect and fate of Ni during aging and thermal-induced phyllomanganate-to-tectomanganate transformation. Geochimica Et Cosmochimica Acta, 2022, 333, 200-215.	3.9	2
96	Speciation and mobility of Zn, Cu and Pb in a truck farming soil contaminated by sewage irrigation. European Physical Journal Special Topics, 2003, 107, 695-698.	0.2	1
97	Reply to the †Comment on "Crystal growth and aggregation in suspensions of Î-MnO2 nanoparticles: implications for surface reactivityâ€â€™ by A. Manceau, Environ. Sci.: Nano, 2018, 5, DOI: 10.1039/C8EN00126J. Environmental Science: Nano, 2018, 5, 2201-2203.	4.3	1
98	Hydration of Na-saturated synthetic stevensite, a peculiar trioctahedral smectite. Clay Minerals, 2020, 55, 229-237.	0.6	0